# Inorganic Chemistry Cite This: Inorg. Chem. 2018, 57, 5585–5596

pubs.acs.org/IC

# Ray-Dutt and Bailar Twists in Fe(II)-Tris(2,2'-bipyridine): Spin States, Sterics, and Fe-N Bond Strengths

Daniel C. Ashley and Elena Jakubikova\*

Department of Chemistry, North Carolina State University, Raleigh, North Carolina 27695, United States

Supporting Information

ABSTRACT: Twisting motions in six-coordinate trischelate transition-metal complexes have long been recognized as a potential reaction coordinate for nondissociative racemization by changing the coordination geometry from octahedral to trigonal prismatic in the transition state. These pathways have been previously established as the Bailar twist (conversion to  $D_{3h}$ symmetry) and the Ray-Dutt twist (conversion to  $C_{2\nu}$  symmetry). Twisting motions have been shown to be associated with changes in spin state and are therefore of relevance not only to thermal isomerization pathways but also to spin-crossover (SCO) and intersystem crossing mechanisms. In this work, density functional theory and complete active space self-consistent field calculations are used to probe the structural and energetic features of idealized

Bailar and Ray-Dutt twisting mechanisms for a model Fe(II) polypyridine complex,  $[Fe(bpy)_3]^{2+}$  (bpy = 2,2'-bipyridine). We find that the energies of the  $D_{3h}$  and  $C_{2\nu}$  trigonal prismatic structures are strongly dependent on spin state, with thermally accessible species only being possible on the quintet surface, enforcing the necessary relationship between SCO and torsional motion. The Ray-Dutt twist on the quintet surface is calculated to proceed with a low barrier, and is likely the preferable twisting mechanism for this complex. We additionally identify a new distorted Bailar twist of C<sub>3h</sub> geometry, which is considerably lower in energy than the idealized  $D_{3h}$  structure due to a combination of both steric and electronic factors. The computational analysis presented herein offers insight into how Fe-N bond strength, interligand steric repulsion, and ligand flexibility can be exploited to influence the rates of different twisting mechanisms and the critical motions involved.

# INTRODUCTION

One of the distinguishing features of first-row transition-metal chemistry is the plethora of accessible electronic states that depending on temperature, pressure, or interaction with light can play a role in reactivity and photochemistry. Application of first-row transition-metal complexes as components of multifunctional materials therefore requires an understanding of how to manipulate spin-state changes, be they through spincrossover (SCO) or light-induced excited spin state trapping (LIESST).2-5 SCO behavior in Fe(II) complexes has been intensely studied for decades, 6,7 and while our understanding of these complexes has grown substantially,8 there are many challenges and questions still remaining.

One issue related to the spin-state energetics of Fe(II) complexes is their potential application in dye-sensitized solar cells (DSSCs), which are promising solar devices that have the potential to be cheaper than traditional silicon cells. 10,11 Unfortunately, unlike more robust Ru(II)-based sensitizers, 12 the photoactive metal-to-ligand charge transfer (MLCT) excited states undergo rapid intersystem crossing (ISC) to low-lying high-spin metal-centered states. 13,14 The shorter lifetimes of the MLCT states decrease the efficiency of the DSSC. While recent studies by Wärnmark 15-20 and Damrauer<sup>21,22</sup> have demonstrated Fe(II) complexes with long-lived

excited states (on the order of ps), rapid ISC is still a typical feature of Fe(II) complexes. To design Fe(II) complexes that can be effectively integrated into DSSCs, it is imperative to increase our understanding of the structural and electronic properties that impact this ISC process. One useful metric in this regard is the determination of  $\Delta E_{\text{O/S}}$ , defined as the difference in energy between the quintet (Q) and singlet (S) states.9,23-27

A great deal of focus has been placed on the role Fe-N stretching motions play in spin-state transitions and nonradiative decay processes in Fe(II) octahedral complexes, since the singlet-to-quintet transition involves population of Fe-L antibonding orbitals, leading to large structural changes.<sup>28-30</sup> While the isotropic breathing mode of Fe complexes is the most relevant reaction coordinate for ISC, other molecular motions also likely contribute to excited-state deactivation. <sup>31–34</sup> Twisting, or torsional motions, about a  $C_3$  (or pseudo- $C_3$ ) axis, such as the Bailar<sup>35</sup> and the Ray-Dutt<sup>36</sup> twists, were originally proposed as mechanisms for racemization of chiral trischelate metal complexes. Both Bailar and Ray-Dutt twists involve conversion of an octahedral  $(O_h)$  structure to a trigonal

Received: March 3, 2018 Published: April 23, 2018



prismatic structure of  $D_{3h}$  or  $C_{2\nu}$  symmetry (Figure 1). Extensive experimental and theoretical work has consistently

Bailar twist 
$$N_1$$
  $N_2$   $N_3$   $N_5$   $N_6$   $N_6$   $N_6$   $N_8$   $N_8$ 

Figure 1. Bailar and Ray-Dutt racemization mechanisms.

shown that there is a strong connection between torsional motions and spin-state changes. This can be rationalized by considering the much weaker ligand field strength of a trigonal prismatic coordination environment (Bailar or Ray-Dutt) compared to octahedral, which leads to significant stabilization of the high-spin states and destabilization of the low-spin states. This results in large barriers (60 to 95 kcal/mol by different estimates) to twisting on the singlet surface of Fe(II) complexes, suggesting that the Bailar/Ray-Dutt twist must be accompanied by SCO. The reverse of this argument has been proposed as well; that is, that effective ISC may be correlated with facile twisting. Therefore, interpreting and quantifying how these motions are coupled to the spin-state manifold may be important for tuning SCO and/or LIESST behavior.

To help address these issues, we employed density functional theory (DFT) and complete active space self-consistent field (CASSCF) calculations to characterize the classic Bailar and Ray-Dutt twist racemization pathways for  $[Fe(bpy)_3]^{2+}$  (bpy = 2,2'-bipyridine). [Fe(bpy)<sub>3</sub>]<sup>2+</sup> has been extensively studied both experimentally and computationally as a prototypical model of iron(II) polypyridine complexes. Surprisingly, to our knowledge, the only iron polypyridine system for which the Bailar and Ray-Dutt twists have been theoretically characterized is [Fe(phen)<sub>3</sub>]<sup>2+</sup> (phen = 1,10-phenanthroline), which was treated with the angular overlap model (AOM)<sup>39</sup> and more recently with semiempirical (PM3) calculations.<sup>49</sup> On the one hand, the AOM calculations indicated the Ray-Dutt twist being higher in energy than the Bailar twist on the singlet surface at ~69 and ~61 kcal/mol, respectively. The PM3 results, on the other hand, predicted these energies at ~75 and ~114 kcal/ mol. The lack of inclusion of steric and interligand interactions in the AOM study makes these conclusions uncertain, as was pointed out in the original publication. The results of both studies, however, are consistent with twisting not occurring on the singlet surface. Other informative DFT studies on Bailar and Ray-Dutt twists have been primarily focused on charged, less sterically crowded ligands such as catecholates, <sup>51</sup> acetylacetonates, <sup>52</sup> and hydroxyquinolates. <sup>53</sup> Fundamental understanding of these twisting motions is a necessary prerequisite for generating multidimensional potential energy surfaces (PESs) that include twisting motions. A previous PES study $^{32}$  on  $[Fe(tpy)_2]^{2+}$  helped illuminate the role of a ligand "rocking" motion in ISC, and it would be useful to apply the same general methodology to  $[Fe(bpy)_3]^{2+}$ .

The results presented in this study suggest that the Ray-Dutt and Bailar twisting mechanisms differ starkly in their energetic viabilities and confirm that spin state indeed has a dramatic effect on which twisting motions are accessible. Furthermore, a new variant of the Bailar twist that involves distortion to lower symmetry ( $C_{3h}$ ), a "dancing" Bailar twist, has been identified. A thorough examination of the molecular and electronic structures of all of these twisted structures demonstrates that spin-state energetics, metal—ligand bond strengths, and interligand steric interactions are all intertwined with each other through torsional motion. Characterization of these pathways and electronic structure features will be important for developing a deeper understanding of the photophysics of Fe(II) polypyridine systems specifically, and transition-metal complexes in general.

# ■ COMPUTATIONAL METHODOLOGY

**DFT Optimizations.** All structures were optimized in vacuum with functional including Grimme's D2 dispersion correction<sup>58</sup> (B3LYP+D2), unless noted otherwise. The SDD basis set and accompanying pseudopotential were used for Fe, 59 and the 6-311G\* basis set<sup>60</sup> was used for all other atoms. An ultrafine integral grid was used for all calculations. Frequencies were calculated for all optimized structures using the harmonic oscillator approximation to verify the nature of the stationary points. The results of these frequency calculations were also used to calculate zero-point energy and entropic corrections to the free energies at 298.15 K and 1.0 atm using standard statistical mechanical conventions. The results discussed in the manuscript itself are the gas-phase electronic energies as opposed to solvated free energies. Energetics calculated with thermochemical and solvation corrections result in the same trends and overall conclusions as the gas-phase electronic energies. Further discussion of these corrections is provided in the Supporting Information (see Table S1).

Several other functionals were employed to evaluate the functional dependence of spin-state energies, barrier heights, and other properties. In most cases, these were used to perform single-point energy calculations on B3LYP+D2 optimized structures, but in some instances structures were reoptimized as well. The additional functionals examined were B3LYP+D3, 61 B3LYP\*, 62-64 B3LYP\*+D2, 65 TPSS, 66 TPSSh, 66-68 BP86<sup>54,69</sup>+D2, M06, 70 M06-L, 71 and APFD. 72 It was found that B3LYP\*+D2 (as well as TPSS and M06-L) offered an excellent agreement with the experimentally estimated  $\Delta E_{O/S_t}$  and hence B3LYP\*+D2 single points were used to report the electronic energy unless noted otherwise. The general conclusions reached by this study are the same regardless of the functional employed. The most significant differences are related to barrier heights on the singlet surfaces and the number of imaginary modes present in some structures. A detailed description of these functional dependence studies can be found in the Supporting Information (see Tables S1 and S2). All of the aforementioned calculations were performed with the Gaussian 09 (G09) software package revision D.01.73 As it was often difficult to force the geometry optimizations to converge to the highly symmetric structures of interest when using G09, NWChem<sup>74</sup> was used in several instances to preoptimize a structure using symmetry constraints, which was then employed as a starting point for subsequent Gaussian optimizations.

The goal of this study was to evaluate the idealized transition-state structures corresponding to the Bailar and Ray-Dutt twists, which are by definition  $D_{3h}$  and  $C_{2\nu}$ . Therefore, geometry optimizations were performed employing symmetry as much as possible within G09, to enforce the ideal point-group symmetry. For simplicity, structures are referred to by their assigned point groups, although in some cases their symmetry was lower than the acceptable default threshold of G09. Regardless, in these cases the structures were qualitatively structurally similar to the desired point group. By forcing the calculations to converge to these highly symmetric local minima, the converged structures often corresponded to higher-order saddle points. When

possible, these additional imaginary modes were removed in subsequent reoptimizations, but for some high-symmetry structures any distortion along these modes necessitated moving the structure to a lower-symmetry point group, as would be expected. A further complication is that the number of imaginary modes was in some cases found to be dependent on the exchange-correlation functional. Specific details on these issues are given in the Supporting Information (see Table S2). Although these high-symmetry species may not always be physically meaningful stationary points, their energies, structures, and chemical properties can still be informative as to the nature of various idealized twisting motions in  $[Fe(bpy)_3]^{2+}$ . If not mentioned otherwise, the reader can assume that all minima have zero imaginary frequencies, and all transition states are proper first-order saddle points.

Potential Energy Surface Scans. One-dimensional PESs along a reaction coordinate corresponding to twisting were calculated for both the Ray-Dutt and Bailar pathways, using combinations of dihedral angles to define the reaction coordinate. For the Bailar pathway, three dihedral angles, one for each pair of bpy ligands, were specified using the coordinating nitrogen atoms on each bpy and constrained to the same value of  $\phi$  (see Figure 2). Only two dihedral angles were constrained for the Ray-Dutt twist, as all three ligands are no longer equivalent in the  $C_{2\nu}$  structure.

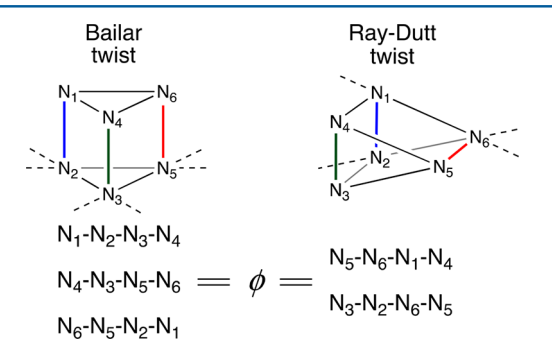


**Figure 2.** Dihedral angles set to  $\phi$  for the Bailar and Ray-Dutt twists. The rotation axes are shown with dashed lines for visualization purposes.

**Multiconfigurational Calculations.** Wave function stability analyses were performed on all B3LYP+D2 optimized structures, and when instabilities were detected, the wave function (and subsequently the molecular geometry) was reoptimized. As will be discussed in detail below, the closed-shell wave functions of the twisted singlet structures were all unstable, and the stable wave functions were heavily spin-contaminated. To verify these DFT results, CASSCF<sup>75–77</sup> calculations were performed on selected structures using Orca 4.0.<sup>78</sup> Calculations with Orca were done using the relativistically contracted<sup>79</sup> all-electron def2-TZVP<sup>80</sup> basis set on all atoms and the Douglas–Kroll–Hess (DKH) relativistic Hamiltonian.<sup>81</sup> Additionally, the RIJCOSX<sup>82,83</sup> approximation and RI-JK auxiliary basis sets<sup>84</sup> were employed to speed up the calculations.

The active space examined was constructed using typical rules for transition-metal complexes and Fe(II) complexes specifically, and idealized diagrams of the working (10,12) active space are shown in Figure 3 for the standard octahedral and  $D_{3h}$  structures. Active spaces for the Ray-Dutt twist were constructed analogously. The active space was kept consistent between all different structures investigated. While the molecular orbital (MO) diagrams 45,85 of twisted structures differ from an octahedral complex, for the case of six d electrons the active spaces are effectively the same, including all five 3d orbitals, six d electrons, and two  $\sigma$ -bonding counterparts to the  $\sigma$ -antibonding orbitals, which are nominally empty in the closed-shell singlet configuration. Additionally, a set of five 4d orbitals was also incorporated to variationally account for dynamic correlation effects. Altogether, this yielded a (10,12) active space. NEVPT2  $^{86-89}$  calculations were performed using the converged CASSCF wave

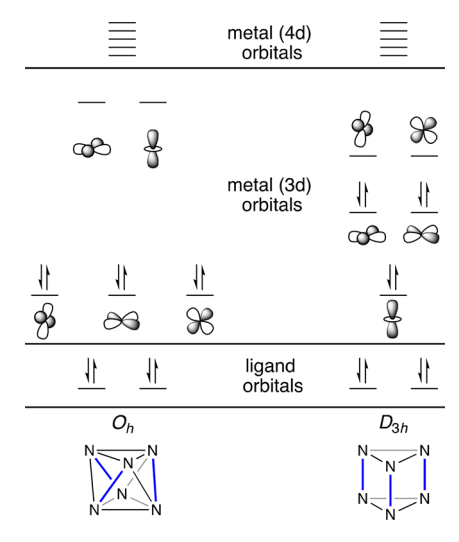


Figure 3. Qualitative MO diagrams of the (10,12) active space for octahedral (left) and Bailar twist (right) geometries.

functions from the (10,12) active space to compare to the DFT results. Recent work from Pierloot<sup>90</sup> has shown that NEVPT2 is generally not an optimal choice for evaluating spin-state energetics, despite the promising early results on other systems, <sup>91,92</sup> and the results of NEVPT2 calculations were therefore mainly used for evaluating relative energetics on a single spin surface.

# ■ RESULTS AND DISCUSSION

The rest of the paper is structured as follows: First a comparison of the calculated results with previous computational and experimental findings is presented. The various twisted structures located with DFT and their relationship to SCO are discussed next. A detailed analysis of these results follows, identifying the electronic and steric contributions to the energetic ordering of the varying twisting pathways. This is followed by an electronic structure analysis of the multiconfigurational character of the twisted structures. Finally, the significance of these results for Fe(II) photochemistry will be discussed.

Comparison of Calculated Spin-State Energetics with Previous Data. Experimentally it is known that  $[Fe(bpy)_3]^{2+}$  is a singlet at room temperature, and its structure has been determined by X-ray crystallography. Table 1 presents a

Table 1. Comparison of Relevant Energetic and Metrical Parameters of  $[Fe(bpy)_3]^{2+}$  Determined Both Experimentally and Computationally

	expt	CASPT2	B3LYP*+D2	B3LYP +D2
$\Delta E_{Q/S}$ [kcal/mol]	$10.0-17.2^{a}$	15.9 <sup>b</sup>	12.7 <sup>c</sup>	6.2
$\Delta E_{\mathrm{T/S}}$ [kcal/mol]		28.6 <sup>b</sup>	19.3 <sup>c</sup>	16.4
Fe-N d [Å]	1.976 <sup>d</sup>	$1.927^{b}$	1.992 <sup>e</sup>	2.000
an c a h	<b>~</b>	6011		

<sup>a</sup>Reference 94. <sup>b</sup>Reference 30. <sup>c</sup>Calculated at the B3LYP+D2 geometry. <sup>d</sup>Reference 93. <sup>e</sup>Optimized with B3LYP\*+D2.

comparison of spin-state energetics for octahedral  $[Fe(bpy)_3]^{2+}$  and average Fe–N distances in its singlet ground state determined using B3LYP\*+D2 and B3LYP+D2 against previously reported experimental and theoretical data. Structurally, there is a good agreement with the experimentally determined Fe–N bond lengths for both DFT methods.

B3LYP+D2 calculations performed in this work indicate that the singlet state is 6.2 kcal/mol higher in energy than the quintet, while the triplet (T) state is 16.4 kcal/mol higher than the singlet state. Previously determined CASPT2 energetics,<sup>30</sup> which agree well with the experimentally 94 estimated range for  $\Delta E_{O/S}$ , are significantly more positive than the B3LYP+D2 calculated values. This is not surprising, as over stabilization of high-spin states is a known shortcoming of B3LYP (and hybrid functionals in general). The use of B3LYP\* with the same parameters for dispersion correction, referred to as B3LYP\*+D2, creates an improvement for  $\Delta E_{Q/S}$  but still underestimates  $\Delta E_{T/S}$ . Both levels of theory predict the correct spin-state ordering as inferred by comparison to the CASPT2 values. While B3LYP+D2 was used for all geometry optimizations reported in this study, given that B3LYP\*+D2 matches the CASPT2 calculated  $\Delta E_{\text{O/S}}$  so well, it was used to calculate all reported electronic energies at these geometries. Any calculations done with other methodologies will be specifically indicated.

Energetic Orderings and Spin-State Preferences for Twisted Structures. Optimized geometries of twisted trigonal prismatic  $[Fe(bpy)_3]^{2+}$  structures are shown in Figure 4, and

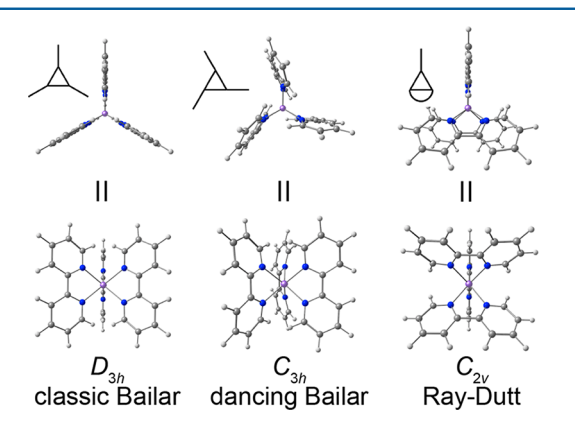


**Figure 4.** Optimized geometries of the three twisted structures. A cartoon next to each structure provides a simple view of the geometry looking down the center of the trigonal prism defined by the coordinated nitrogen atoms.

Table 2. Calculated Electronic Energies for  $[Fe(bpy)_3]^{2+}$  in Twisted Geometries<sup>a</sup>

	$D_3$	$D_{3h}$	$C_{3h}$	$C_{2\nu}$
singlet	0.0	83.8	65.0	48.9
triplet	19.3			43.0
quintet	12.7	51.4	36.8	25.2

<sup>a</sup>Note that the pseudo-octahedral structures belong to the  $D_3$  point group. All values are in kcal/mol.

calculated energetics are provided in Table 2, with all values being reported relative to the pseudo-octahedral  $(D_3)$  complex in the singlet state. The classic Bailar structure is much higher in energy than the Ray-Dutt structure for both the singlet and quintet by  $\sim 30$  and  $\sim 20$  kcal/mol, respectively. With the exception of the  $C_{2\nu}$  Ray-Dutt structure, the highly symmetric structures could not be optimized for the triplet state, as they always collapsed back to the octahedral ground state, likely due to the expected first order Jahn–Teller distortions. Moreover,

the triplet Ray-Dutt structure reported in Table 2 is not a proper first-order saddle point. The triplet will likely pass through a torsional pathway similar to the ones examined here but distorted to some lower symmetry. In the current work, the analysis is focused on the singlet and quintet spin states due to these additional complexities.

The calculated relative ordering of Ray-Dutt and Bailar twists varies from method to method 39,49 and from system to system. 51-53 The two are usually very close in energy for less sterically crowded ligands. For the Ray-Dutt and Bailar twist of  $[Fe(phen)_3]^{2+}$ , it was predicted that the former was ~10 kcal/ mol higher in energy by AOM calculations, while PM3 calculations predicted that the Bailar was ~40 kcal/mol higher in energy than the Ray-Dutt. The DFT results in Table 2 are surprisingly similar to the PM3 results, though the actual barrier heights predicted by PM3 were much larger than those reported in Table 2. It is possible, however, that DFT is underestimating the barrier height on the singlet surface as discussed in more detail below. The disagreement with AOM could be interpreted as suggesting that interligand interactions for trispolypyridine complexes play a critical role in determining the preference for one twisting mechanism over another.

The Bailar twist is classically defined as a trigonal prism of  $D_{3h}$  symmetry (see Figure 1); however, this high-symmetry structure is always calculated as a higher-order saddle point with all functionals investigated; that is, it possesses numerous imaginary modes (as many as nine), meaning that the Bailar twist "transition state" is not a physically meaningful point on the potential energy surface. By allowing the  $D_{3h}$  structure to relax along these additional imaginary modes, the optimization converges to a different trigonal prismatic Bailar-like geometry that still possesses three-fold symmetry but is now  $C_{3h}$ . The new  $C_{3h}$  structure is lower in energy by ~15-20 kcal/mol for both spin states (see Table 2). Although the number of imaginary modes is method-dependent (see Table S2), in most cases these structures now only possess one imaginary mode. As shown in Figure 4, the bpy ligands in this  $C_{3h}$  structure are partially folded, and the contact nitrogens are no longer pointing directly at the metal center. Given the elegant "spiral" shape of this structure we denoted it the "dancing Bailar" twist. 95 To the best of our knowledge, this structure has not been reported before. The  $D_{3h}$  structure will now be referred to as the "classic Bailar" to help distinguish the two. These calculations show that if  $[Fe(bpy)_3]^{2+}$  undergoes twisting along a Bailar-like pathway, it will also undergo significant distortion/ folding of the bpy ligands. Note that, although the dancing Bailar does provide a lower-energy Bailar-like twist, it is still not lower in energy than the Ray-Dutt twist.

The quintet states are always significantly lower in energy than the singlets for all twisted structures. For example, for the dancing Bailar twist, the quintet is ~30 kcal/mol lower in energy than the singlet, and for the Ray-Dutt twist, the quintet is ~25 kcal/mol lower. While hybrid functionals are known to overstabilize the quintet states, B3LYP\*+D2 provides a relatively accurate  $\Delta E_{\mathrm{Q/S}}$  for the octahedral complex (see Table 1). However, because of the large structural differences between the different twisted and octahedral structures, it is not clear if the functional dependence will be of the same magnitude. This notwithstanding, the calculated energy differences are large enough that these results are likely qualitatively accurate. It is worth noting that there are two other functionals that also match the experimental spin-state energetics with similar accuracy as B3LYP\*+D2, namely,

M06-L and TPSS, and that they also exhibit very similar energetics as B3LYP\*+D2 for all of the other structures/spin states considered here. The results in Table 2 then demonstrate that torsional motions are strongly associated with spin-state transitions, as the ground state changes from the singlet to quintet for each twisting mechanism. This conclusion is in good agreement with what has been historically proposed for the necessary dependence of twisting on SCO. <sup>39,40</sup>

The quintet Ray-Dutt twist is unambiguously the lowest energy of all the twisted structures;  $\sim$ 25 kcal/mol higher in energy than the ground-state  $D_3$  singlet and only  $\sim$ 13 kcal/mol above the  $D_3$  quintet. This means that once the quintet state surface is accessed, be it through thermal SCO or LIESST, there will be a rapid, nondissociative racemization pathway available for  $[Fe(bpy)_3]^{2+}$ . It is important to realize that the Ray-Dutt transition state is also the only one that is reasonably accessible at room temperature (assuming  $\sim$ 20–25 kcal/mol being an upper limit on the activation energy).

Table 3 lists the average Fe-N bond lengths for all considered structures in both the singlet and quintet states.

Table 3. Average Fe-N Bond Lengths for Twisted Structures<sup>a</sup>

	$D_3$	$D_{3h}$	$C_{3h}$	$C_{2\nu}$
Fe-N d (S)	2.000	2.338	2.223	2.091/2.212
Fe-N d (Q)	2.193	2.368	2.272	2.207/2.249

<sup>&</sup>quot;All values are given in angstroms. For the  $C_{2\nu}$  structure the bpy that is orthogonal to the other two has a shorter bond length and is listed first.

As expected, the singlets always have shorter Fe—N bonds than the quintets, due to their minimization of the occupation of strongly antibonding orbitals. Notably, all of the twisted structures possess much longer Fe—N bonds than the  $D_3$  structures. This results from a significant weakening of the metal—ligand bonds during twisting. The Fe—N bond lengths for the quintet Ray-Dutt are by far the most similar to their respective octahedral bond lengths, possibly an indication of why this is the lowest-energy twisting pathway.

Figure 5 reinforces the necessity of SCO in preliminary onedimensional PESs for  $[Fe(bpy)_3]^{2+}$ , where twisting is controlled by fixing the dihedral angles between pairs of bpy ligands,  $\phi$ (see Figure 2). After only an intermediate degree of twisting

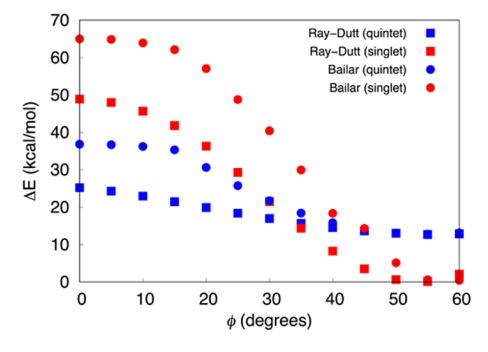


**Figure 5.** Preliminary one-dimensional twisting PESs for the Ray-Dutt ( $\blacksquare$ ) and dancing Bailar ( $\blacksquare$ ) twists in  $[Fe(bpy)_3]^{2+}$ . The quintet surfaces are colored blue, while the singlets are colored red. Energies are reported relative to the fully optimized  $D_3$  singlet. Note that in the Bailar scans the structure naturally relaxes to the dancing Bailar twist for both spin states.

(~20–25°), the quintet becomes the preferred spin state for both the Bailar and Ray-Dutt twists. It is reasonable to expect that the minimum energy crossing points (MECPs) between the various spin surfaces will also be located at this intermediate degree of twisting. While these one-dimensional PESs should be interpreted cautiously, it is encouraging that the surfaces cross at relatively low energies (~10–15 kcal/mol) relative to the singlet ground state. Since torsional motions are strongly connected to SCO, it is possible that ligand twisting could have a significant impact on spin-surface crossing rates. Of course, any interpretation of the SCO behavior of  $[Fe(bpy)_3]^{2+}$  complex will necessarily rely on locating the MECPs on the PESs, which will be done in a follow-up study.

Electronic Versus Steric Factors in Determining the Lowest-Energy Twisting Pathways. That the classic Bailar twist is not a legitimate pathway for  $[Fe(bpy)_3]^{2+}$  was surprising, and the demonstration that a Bailar twist can still occur through the dancing Bailar showed that the flexibility of the bpy ligand plays a role in dictating the energetics of torsional motion. Figure 6 shows space-filling models of the

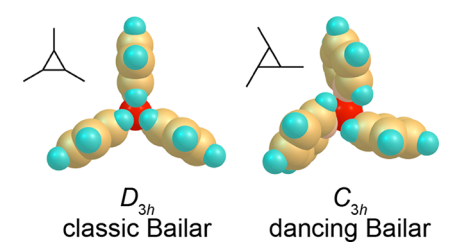


**Figure 6.** Space-filling models of the classic Bailar twist and the dancing Bailar twist viewed along the  $C_3$  rotation axis.

classic and dancing Bailar structures viewed down their  $C_3$  rotational axes. In the classic Bailar twist, the hydrogens at the 6,6' positions of each bpy are pointing directly into the center of the prism and therefore directly at each other. Folding of the bpy ligands and canting them with respect to the metal center in the dancing Bailar twist pivots them away from each other, thereby decreasing the steric interactions. Despite this somewhat obvious explanation, sterics need not be the only factor influencing which twisting mechanism will predominate. As was intimated earlier by the varying Fe–N bond lengths in the twisted structures, there could be a significant electronic/bonding component as well.

To probe this in more detail, the classic Bailar twist was systematically converted into either the dancing Bailar or Ray-Dutt twist in the two chemically meaningful steps shown in Figure 7 with calculated values provided in Table 4. The results discussed here are calculated with B3LYP+D2, but they are not expected to show any significant functional dependence (no energy differences between structures of different multiplicities are considered). The first step involves distorting the bpy ligands to their final, folded form found in the twisted structure but without changing the Fe-N bond lengths ( $\Delta E_1$ ). The second step then relaxes the bond lengths to their shorter, final lengths ( $\Delta E_2$ ). To investigate interligand interactions on their own, the same procedure was also performed without the metal ion keeping the ligands in the same geometry as in the metal complex ( $\Delta EL_1$  and  $\Delta EL_2$ ). The sum of the two steps is referred to as  $\Delta E$  and  $\Delta E$ L for the whole complex and only the ligands, respectively. If interligand sterics are all that dictates a preference for one twisting mechanism over another, then  $\Delta E$ 

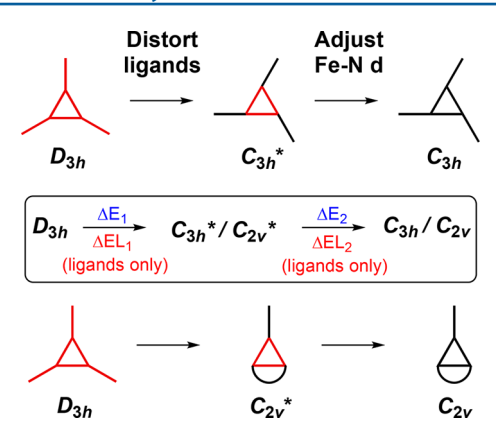


**Figure 7.** Stepwise interconversion of the classic Bailar into the dancing Bailar and Ray-Dutt twists.

should be well-approximated by  $\Delta EL$ . This is not the case, however, with  $\Delta EL$  never accounting for much more than  $\sim$ 50% of  $\Delta E$ .

 $\Delta E_1$  is always a stabilizing feature, signifying that relief of steric strain by rotating the 6 and 6' hydrogens outward does contribute to the greater stability of the dancing Bailar as initially suspected.  $\Delta EL_1$  is similar in size, emphasizing the interligand origins of this step.  $\Delta EL_1$  is usually slightly more favorable, however, because  $\Delta E_1$  also contains an unfavorable decrease in overlap of metal and ligand orbitals. The most critical information is obtained from  $\Delta E_2$ , which is also always negative and non-negligible but smaller than  $\Delta E_1$ .  $\Delta E_2$ represents the energy released by forming stronger, shorter Fe-N bonds in the twisted structure. Now compare  $\Delta E_2$  with  $\Delta EL_2$ :  $\Delta EL_2$  is always a positive quantity, indicating unfavorable interactions due to the contraction of the Fe-N bonds, which forces the bpy ligands closer together and serves to increase steric repulsion. The steric penalty incurred by shortening the Fe-N bonds does not cancel the stabilizing steric effect of  $\Delta E_1$  (as revealed by comparing  $\Delta EL_1$  and  $\Delta EL_2$ ), but it significantly diminishes the release of steric strain involved, primarily for the Bailar twists and less so for the Ray-Dutt twists.

It can be concluded that, although the folding and rotating of the bpy ligands to relieve steric penalties is energetically important, in the final twisted structures some of this steric strain has been regained due to the shorter Fe–N bonds, and therefore a major component of  $\Delta E$  arises from changes in Fe–N bond strength; again note how much more favorable  $\Delta E$  is compared to  $\Delta E$ L. Steric interactions from the interacting bpy ligands are still very important, however, as they are essentially what forces the Fe–N bonds to be long and weak in the first place. By folding the ligands out the steric strain is relieved, but only temporarily, as the ligands will now form stronger bonds and bring some additional steric strain back.

These conclusions are true regardless of spin state, although the effects are less pronounced for the quintet, and the contribution of sterics becomes more pronounced, a natural consequence of the weaker Fe—N bonds in all of the quintet structures. This demonstrates an important point: in this case the Fe—N bonds are weakened by going from the singlet to the quintet, therefore making sterics a more dominant factor in controlling  $\Delta E$ , but this result could also be achieved by using ligands that naturally make weaker bonds to Fe (or stronger for the opposite effect). Ligand design then can be used in multiple ways (sterically or electronically) to influence torsional pathways and spin state changes.

Similar results for the stepwise conversion of the classic Bailar to Ray-Dutt structures (see Table 4) also provide an explanation for why the Ray-Dutt structures are even lower in energy than the dancing Bailar twist. By rotating one bpy ligand 90°, the Ray-Dutt structure manages to avoid steric clashes with this rotated ligand (or at least clashes of the same magnitude), which allows the rotated bpy ligand to move even closer to the Fe center and enables shorter, stronger bonds than the dancing Bailar as shown in Table 3. The two bpy ligands that did not rotate also form stronger bonds, as evidenced by their bond lengths, which are similar to the lengths in the dancing Bailar. All of these bond lengths are longer relative to the  $D_3$  ground state, however, showing that the Fe-N bonding is relatively weaker in the Ray-Dutt twist. Note that, although the trends in the Ray-Dutt twist are similar to those in the dancing Bailar (see Table 4), the magnitudes of the energy changes have approximately doubled for both  $\Delta E_1$  and  $\Delta E_2$ , indicating that the Ray-Dutt twist is lower in energy than the dancing Bailar due to both a greater minimization of unfavorable steric interactions and an increase in metal-ligand bond strength.

Another consideration in determining the relative energetics of the twisted structures is the pseudo Jahn-Teller effect (PITE), which induces molecular distortions to lower symmetry due to interactions between the ground and excited state(s) mediated by vibronic coupling. 96-98 The PITE will only significantly contribute to a distortion if the energy difference between the two states is small enough, which typically can be related to small highest occupied molecular orbital (HOMO)-lowest unoccupied molecular orbital (LUMO) gaps. Indeed, one of the key features of the twisted structures examined here is that they have much weaker ligand fields than the  $D_3$  complex, resulting in low-lying high-spin states and significant multiconfigurational behavior in the singlet state (see below). These behaviors are very consistent with the small energy gaps between states that are necessary for the PJTE, and it is quite possible that it plays some role in twisting motion. This is in no way contradictory to the effects described above, but rather it would be an additional factor behind these transformations. Deconvoluting the PJTE from other electronic or steric effects is, however, nontrivial as shown

Table 4. Calculated Values<sup>a</sup> for the Stepwise Interconversions of Twisted Structures Shown in Figure 7

multiplicity	structure	$\Delta E_1$	$\Delta E \mathrm{L}_1$	$\Delta E_2$	$\Delta E \mathrm{L}_2$	$\Delta E$	$\Delta E L$
singlet	$C_{3h}$	-9.5	-13.4	-8.0	6.2	-17.5	-7.2
	$C_{2\nu}$	-17.2	-18.2	-15.7	6.4	-33.0	-11.8
quintet	$C_{3h}$	-8.2	-11.7	-5.6	4.2	-13.8	-7.5
	$C_{2\nu}$	-16.0	-16.0	-9.5	3.9	-25.5	-12.1

<sup>&</sup>lt;sup>a</sup>Calculated using B3LYP+D2; in kcal/mol.

in other computational studies, <sup>96</sup> and it is outside the scope of this study.

Multiconfigurational Nature of the Singlet Twisted Structures. An interesting feature of the singlet twisted structures is their multiconfigurational character. While the quintet states resemble typical Fe(II) high-spin states based on Mulliken spin, spin contamination, and natural orbital occupations that are close to integer values, the singlets are much more complex. Initially, all the Bailar and Ray-Dutt twist structures were calculated as closed-shell singlets, but their wave functions were determined to be unstable. Wave function and geometry reoptimizations yielded much lower energy structures with drops in energy of 20.6, 28.0, and 38.7 kcal/mol for the  $C_{2\nu}$ ,  $C_{3h}$ , and  $D_{3h}$  structures, respectively. These new structures had highly spin-contaminated wave functions (Table 5). The high values of  $\langle S^2 \rangle$  are indicative of broken symmetry

Table 5. Diagnostic Electronic Structure Parameters from Singlet CASSCF (10,12) and B3LYP+D2 Calculations<sup>a</sup>

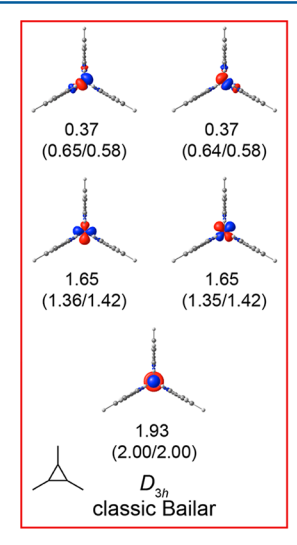
	$D_3$	$D_{3h}$	$C_{3h}$	$C_{2\nu}$
$\langle S^2 \rangle$	0.00	1.75	1.65	1.45
dominant CSF %	93%	66%	72%	78%

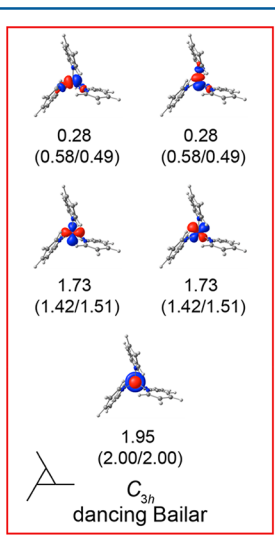
"For DFT  $\langle S^2 \rangle$  is reported, which should be zero in the absence of any spin contamination. The percent contribution of the dominant configuration state function (CSF) to the overall wavefunction is indicated for CASSCF. All values in this table are calculated with def2-TZVP on all atoms.

(BS) solutions that involve occupation of the antibonding  $\sigma^*$  orbitals; that is, these calculations imply that the electronic structure will become significantly multiconfigurational during twisting on the singlet surface. While direct comparison is difficult, Purcell noted in the earlier AOM study of [Fe-(phen)<sub>3</sub>]<sup>2+</sup> that inclusion of configuration interaction terms resulted in lowering the energy of the singlet Ray-Dutt twist by 21 kcal/mol, in remarkable agreement with what is seen here (although it should be noted that geometry reoptimization in our case contributed ~5 kcal/mol of the stabilization).<sup>39</sup>

The increased multiconfigurational character of these geometries makes chemical sense, as twisting is associated with elongated Fe-N bond lengths and consequently a weaker ligand field. That being said, open-shell singlets centered on a single metal center are not common, and there was a concern that this solution was an artifact of the BS approximation. Therefore, CASSCF calculations were done on the optimized structures to confirm the nature of the BS-DFT wave functions. Natural orbitals and their occupation numbers from the CASSCF calculations are shown in Figure 8 and are qualitatively highly similar to unrestricted natural orbitals obtained from the DFT Kohn-Sham wave functions. Table 5 also lists the weight of the dominant configuration state function (CSF) in the CASSCF wave function, which was always closed-shell. It is quite clear from the CASSCF calculations that the twisted structures are significantly more multiconfigurational than the octahedral structure, with the dominant CSF comprising 93% and 66% of the total wave function for the octahedral and classic Bailar structures, respectively. This is also consistent with the magnitude of deviation of the natural orbital occupation numbers from integer values in the CASSCF calculations, which could be as much as 0.37 for the classic Bailar (Figure 8) but much smaller, never more than 0.04, for the octahedral structure. The degree of multiconfigurational character in the CASSCF wave functions also tracks well with the spin contamination in the DFT calculations, which shows that DFT is at least qualitatively correctly reporting on the changes in complex electronic structure of these species.

This multiconfigurational character is important to analyze for several reasons. From a practical standpoint, it indicates that any attempts to explore the PES of twisting motions for the singlet states will involve conversion from a closed-shell to open-shell singlet electronic structure, which should influence the choice of computational methodology. Chemically speaking, the appearance of multiconfigurational character further underscores the significant effect twisting has on the ligand field strength of  $[Fe(bpy)_3]^{2+}$  and, consequently, on the spin-state





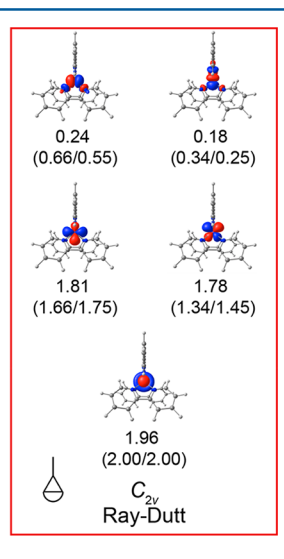


Figure 8. Natural orbitals for the singlet states of twisted structures as determined from CASSCF (10,12) calculations. Only the metal 3d orbitals are shown, as they are the most illustrative of the changes in electronic structure. CASSCF natural orbital occupation numbers are provided, and analogous B3LYP+D2 and BP86+D2 occupation numbers from unrestricted natural orbitals are given sequentially in parentheses. These DFT calculations were done with Orca using the exact same basis set as the CASSCF calculations they are being compared to. Note that the orbitals are ordered as expected for the Bailar twist<sup>45,85</sup> for all three complexes purely for aesthetic reasons. Isovalue =  $0.04 \text{ e/A}^3$ .

energetics. Another interesting feature is that the largest multiconfigurational character is associated with the least-stable (highest-energy) structures, which draws an additional connection between multiconfigurational character being strongly associated with weaker ligand field strength and therefore weaker Fe—N bonding. This corroborates the argument that the Fe—N bond strength is an important factor in determining the energetic preference of one twisting pathway over another.

The comparison between the CASSCF and DFT results offers some additional insights. While the methodologies agree on the overall features of the system, the BS-DFT calculations significantly overestimate the degree of polyradical character, as can be seen by comparing the natural orbital occupation numbers of the CASSCF calculations with those determined from unrestricted natural orbitals generated from the B3LYP+D2 and BP86+D2 Kohn—Sham wave functions (Figure 8). Hybrid functionals have been previously shown to overestimate diradical character when compared to multireference calculations. <sup>99–103</sup> In this case, however, a pure functional (BP86) still overestimates the polyradical behavior relative to CASSCF, although slightly less so than B3LYP+D2.

The electronic structure of the singlet states may also have a significant effect on calculated barrier heights and their functional dependence. While the calculated barrier heights on the quintet surface do not vary by more than  $\sim \! 10 \text{ kcal/mol}$  across the range of examined functionals (usually less than 4 kcal/mol), on the singlet surface they vary by as much as  $\sim \! 27 \text{ kcal/mol}$ . Figure 9 shows a strong relationship between the spin

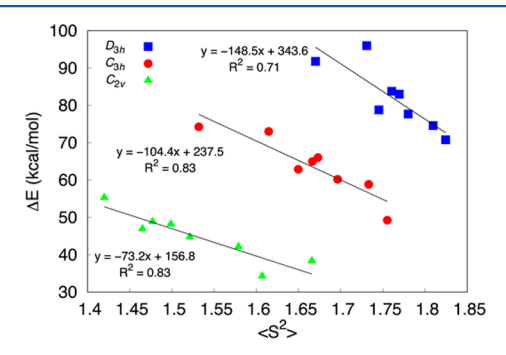


Figure 9. Singlet twisted structure energies as a function of  $\langle S^2 \rangle$  for various functionals. All energies were calculated using the B3LYP+D2 optimized structures and the basis sets described in the Methodology section. Details on which functionals were considered and a similar analysis for the quintet energies are provided in the Supporting Information.

contamination and barrier height, where increasing multiconfigurational character leads to a lower calculated energy. Note that such a relationship is not present for the quintet states (see Figure S1). As the CASSCF results show that the BS-DFT results are always overestimating the radical character, this may indicate that the barrier heights calculated with BS-DFT are systematically being underestimated. Figure 9 also shows that the sensitivity of the barrier height to the multiconfigurational character of the wave function (as indicated by the magnitude of the slope) is largest for  $D_{3h}$  and smallest for  $C_{2\nu}$  structures, which is consistent with the more inherently multiconfigurational structure showing the greatest functional dependence.

Supporting this interpretation is that multireference perturbation theory calculations (NEVPT2) do predict much

higher barriers on the singlet surface than any examined DFT method, while yielding barrier heights similar to those calculated with DFT on the quintet surface (see Table S1). Although NEVPT2 has been shown recently to be a poor choice for calculating spin-state energies, 90 there is no reason to expect that it would fail to accurately predict relative energetics within a particular spin state. In fact, NEVPT2 has been shown to perform well for predicting barrier heights, although this conclusion was reached for small, main-group molecules and may not be applicable to our system. 104 Overall, this analysis shows that used as is, DFT is most likely underestimating the energies of twisted structures on the singlet surface by overemphasizing their multiconfigurational character. Application of spin-projection techniques to calculations on twisted structures could mitigate some of these problems, but this is beyond the scope of the present study.

Several of the conclusions reached from the CASSCF/BS-DFT study for  $[Fe(bpy)_3]^{2+}$  may be applicable to other systems. Most importantly, the multiconfigurational character of a particular structure will likely be proportional to the degree of twisting, all else being equal. Twisting will always induce intramolecular strain that weakens bonds, leading to more accessible high-spin states and multiconfigurational low-spin states. The functional dependence and spin contamination issues appear to track with multiconfigurational character as well, but more examples are needed to verify this. The extent of multiconfigurational character present in a given twisted structure will, however, not be necessarily consistent across systems. For example, while Fe(II) and Co(III) are isoelectronic, the stronger and shorter bonds of Co(III) will have a different sensitivity to twisting, resulting in different magnitudes of multiconfigurational effects across their respective complexes.

Relevance of Twisting to ISC. To ascertain how the twisted structures may play a role in MLCT deactivation, the energies of the twisted structures should be considered relative to the lowest-energy singlet MLCT state, which can be estimated as 55–58 kcal/mol<sup>30,105,106</sup> above the singlet ground state (or even less, 48.4 kcal/mol, if the onset of the MLCT band is taken as the estimate for the excited state as opposed to the band maximum<sup>30</sup>). With the B3LYP\*+D2 set of data, the dancing Bailar and Ray-Dutt twist structures are 65.0 and 48.9 kcal/mol on the singlet surface and 36.8 and 25.2 kcal/mol on the quintet surface, respectively. The twisted singlet structures are within 10–15 kcal/mol of the initially formed <sup>1</sup>MLCT state using the DFT energies. With the NEVPT2 energies, however, the energy of these structures increases to 85.2 and 62.6 kcal/ mol on the singlet surface (given the obvious fault in NEVPT2 for calculating spin-state splitting the quintet energies will be ignored for the present discussion). Specific numbers aside, what these calculations indicate is that these twisted structures are in an energy regime where they may be thermodynamically accessible from the excited MLCT state given the spread in values among DFT functionals and NEVPT2. From a thermodynamic standpoint then, this means that twisting could represent an important component of the molecular motion involved in ISC. What will ultimately be most important is not the thermodynamics, but rather the kinetic viability of twisting.

It is likely that the singlet MLCT surface will resemble the singlet surface, which consequently will make twisted singlet MLCT structures very high in energy and not accessible before ISC can occur. Even if this is true, this does not necessarily

mean torsional motion is unimportant or impossible for ISC. The goal of this study was to carefully analyze the dancing Bailar and Ray-Dutt transition states to provide insight into the electronic structure changes that occur during torsional motion, but these transition states do not necessarily need to be accessed during ISC. The actual crossing point will likely only involve a modest degree of twisting in combination with bondstretching. A similar point was made in the AOM study mentioned previously.<sup>39</sup> Additionally, recall that the onedimensional PESs in Figure 5 showed the spin surfaces crossing after only moderate twisting had occurred and at much lower energies than the transition states themselves. It is important to note that the conclusions reached in this work based on the fully twisted structures will almost certainly be applicable for small or moderate twisting motions along the reaction coordinate.

Another point that has not been addressed is that facile spin-state switching requires significant spin-orbit coupling (SOC) between the states at hand. One of the more impactful consequences of SOC is that the calculated SOC constants for the singlet MLCT to triplet conversion are larger than the singlet MLCT to quintet conversion, and this has been used as evidence that the triplet states might be important intermediates in the ISC process. As mentioned previously, the triplet states will be more easily handled in a full PES study, where additionally it will be possible to identify what effect (if any) twisting has on SOC.

Without detailed multidimensional PESs, however, it is difficult to confidently calculate where spin-surface crossings between the MLCT and MC states occur when torsional motion is an explicit reaction coordinate. Determining this will involve a thorough analysis of the MLCT and MC surfaces as a function of torsional motion and bond stretching. Using the data generated in this study, we can now move forward and construct said PESs as we have done in previous work<sup>32</sup> to properly understand how twisting motion does, or does not play a role, in ISC for [Fe(bpy)<sub>3</sub>]<sup>2+</sup>.

# CONCLUSIONS

This work presents a thorough analysis of the iconic Bailar and Ray-Dutt racemization pathways in  $[Fe(bpy)_3]^{2+}$  using DFT and CASSCF calculations. The Ray-Dutt twist is found to be the lowest in energy, and an alternative Bailar-like twist of  $C_{3h}$  symmetry, denoted as the "dancing Bailar" twist, is a preferred twisting pathway to the classic Bailar twist. The CASSCF and BS-DFT calculations suggest that all twisted singlet structures possess significant multiconfigurational character, likely due to the distorted structures having much weaker ligand field strengths.

All twisting pathways investigated are energetically more accessible on the quintet surface, emphasizing that torsional motion and spin-state energetics are strongly connected. While the twisting will not occur at room temperature on the singlet surface, the Ray-Dutt twist on the quintet surface is only  $\sim 10-15~\rm kcal/mol$  higher in energy than the octahedral quintet, suggesting that torsional motion can occur, but only if it is accompanied by SCO, confirming predictions made in previous work. <sup>39,40</sup> The low quintet barrier also indicates that torsional motion may be relevant to LIESST studies where the quintet state is formed photochemically.

Analysis of the different twisting structures showed how Fe-N bond strengths and steric interactions between ligands can influence barrier heights in addition to spin-state energetics.

The twisted structures examined here can then be used as guides for how torsional motion is connected to spin-state energies and to determine what molecular features enhance or diminish the rate of twisting. Our calculations suggest that designing complexes with larger interligand steric interactions, stronger Fe–N bonds, and rigid ligands that are resistant to folding can raise the barrier for twisting. Further work involving multidimensional PESs of all possible spin states is needed to fully understand the role of twisting in ISC for Fe(II) complexes, but the results determined in this study already offer an insight into how torsional motion may impact excited-state lifetimes in transition-metal complexes.

#### ASSOCIATED CONTENT

### S Supporting Information

The Supporting Information is available free of charge on the ACS Publications website at DOI: 10.1021/acs.inorg-chem.8b00560.

Additional discussion on the method dependence of calculated energetics; additional discussion on the method dependence of the nature of the reported stationary points; raw calculated energies for all species considered (PDF)

Cartesian coordinates of all optimized structures (XYZ)

# AUTHOR INFORMATION

# **Corresponding Author**

\*E-mail: ejakubi@ncsu.edu.

ORCID

Elena Jakubikova: 0000-0001-7124-8300

Notes

The authors declare no competing financial interest.

# ACKNOWLEDGMENTS

This work was supported by the National Science Foundation (NSF) Grant No. CH-1554855. This work used the Extreme Science and Engineering Discovery Environment (XSEDE) Bridges at the Pittsburgh Supercomputing Center through Allocation No. TG-CHE170031. XSEDE is supported by the NSF ACI-1548562. <sup>107</sup>

# REFERENCES

- (1) Ashley, D. C.; Jakubikova, E. Ironing out the Photochemical and Spin-Crossover Behavior of Fe(II) Coordination Compounds with Computational Chemistry. *Coord. Chem. Rev.* **2017**, *337*, 97–111.
- (2) Gamez, P.; Costa, J. S.; Quesada, M.; Aromi, G. Iron Spin-Crossover Compounds: From Fundamental Studies to Practical Applications. *Dalton Trans.* **2009**, 7845–7853.
- (3) Sato, O.; Tao, J.; Zhang, Y. Z. Control of Magnetic Properties through External Stimuli. *Angew. Chem., Int. Ed.* **2007**, *46*, 2152–2187.
- (4) Bousseksou, A.; Molnár, G.; Matouzenko, G. Switching of Molecular Spin States in Inorganic Complexes by Temperature, Pressure, Magnetic Field and Light: Towards Molecular Devices. *Eur. J. Inorg. Chem.* **2004**, 2004, 4353–4369.
- (5) Gaspar, A. B.; Ksenofontov, V.; Seredyuk, M.; Gütlich, P. Multifunctionality in Spin Crossover Materials. *Coord. Chem. Rev.* **2005**, 249, 2661–2676.
- (6) Gütlich, P.; Garcia, Y.; Goodwin, H. A. Spin Crossover Phenomena in Fe(II) Complexes. *Chem. Soc. Rev.* **2000**, *29*, 419–427. (7) Gütlich, P.; Gaspar, A. B.; Garcia, Y. Spin State Switching in Iron Coordination Compounds. *Beilstein J. Org. Chem.* **2013**, *9*, 342–391.

(8) Halcrow, M. A. Spin-Crossover Materials: Properties and Applications; John Wiley & Sons, Incorporated: Chichester, United Kingdom, 2013.

- (9) Jakubikova, E.; Bowman, D. N. Fe(II)-Polypyridines as Chromophores in Dye-Sensitized Solar Cells: A Computational Perspective. *Acc. Chem. Res.* **2015**, *48*, 1441–1449.
- (10) Meyer, G. J. Molecular Approaches to Solar Energy Conversion with Coordination Compounds Anchored to Semiconductor Surfaces. *Inorg. Chem.* **2005**, *44*, 6852–6864.
- (11) Hagfeldt, A.; Boschloo, G.; Sun, L.; Kloo, L.; Pettersson, H. Dye-Sensitized Solar Cells. *Chem. Rev.* **2010**, *110*, 6595–6663.
- (12) Ardo, S.; Meyer, G. J. Photodriven Heterogeneous Charge Transfer with Transition-Metal Compounds Anchored to TiO<sub>2</sub> Semiconductor Surfaces. *Chem. Soc. Rev.* **2009**, *38*, 115–164.
- (13) Monat, J. E.; McCusker, J. K. Femtosecond Excited-State Dynamics of an Iron(II) Polypyridyl Solar Cell Sensitizer Model. *J. Am. Chem. Soc.* **2000**, 122, 4092–4097.
- (14) Zhang, W.; Alonso-Mori, R.; Bergmann, U.; Bressler, C.; Chollet, M.; Galler, A.; Gawelda, W.; Hadt, R. G.; Hartsock, R. W.; Kroll, T.; Kjaer, K. S.; Kubicek, K.; Lemke, H. T.; Liang, H. W.; Meyer, D. A.; Nielsen, M. M.; Purser, C.; Robinson, J. S.; Solomon, E. I.; Sun, Z.; Sokaras, D.; van Driel, T. B.; Vanko, G.; Weng, T. C.; Zhu, D.; Gaffney, K. J. Tracking Excited-State Charge and Spin Dynamics in Iron Coordination Complexes. *Nature* **2014**, *509*, 345–348.
- (15) Liu, Y.; Persson, P.; Sundström, V.; Wärnmark, K. Fe N-Heterocyclic Carbene Complexes as Promising Photosensitizers. *Acc. Chem. Res.* **2016**, *49*, 1477–1485.
- (16) Fredin, L. A.; Pápai, M.; Rozsályi, E.; Vankó, G.; Wärnmark, K.; Sundström, V.; Persson, P. Exceptional Excited-State Lifetime of an Iron(II)—N-Heterocyclic Carbene Complex Explained. *J. Phys. Chem. Lett.* **2014**, *5*, 2066–2071.
- (17) Liu, Y.; Harlang, T.; Canton, S. E.; Chabera, P.; Suarez-Alcantara, K.; Fleckhaus, A.; Vithanage, D. A.; Goransson, E.; Corani, A.; Lomoth, R.; Sundström, V.; Wärnmark, K. Towards Longer-Lived Metal-to-Ligand Charge Transfer States of Iron(II) Complexes: An N-Heterocyclic Carbene Approach. *Chem. Commun.* **2013**, *49*, 6412–6414.
- (18) Harlang, T. C. B.; Liu, Y.; Gordivska, O.; Fredin, L. A.; Ponseca, C. S., Jr; Huang, P.; Chábera, P.; Kjaer, K. S.; Mateos, H.; Uhlig, J.; Lomoth, R.; Wallenberg, R.; Styring, S.; Persson, P.; Sundström, V.; Wärnmark, K. Iron Sensitizer Converts Light to Electrons with 92% Yield. *Nat. Chem.* **2015**, *7*, 883–889.
- (19) Chábera, P.; Kjaer, K. S.; Prakash, O.; Honarfar, A.; Liu, Y.; Fredin, L. A.; Harlang, T. C. B.; Lidin, S.; Uhlig, J.; Sundström, V.; Lomoth, R.; Persson, P.; Wärnmark, K. Feii Hexa N-Heterocyclic Carbene Complex with a 528 ps Metal-to-Ligand Charge-Transfer Excited-State Lifetime. *J. Phys. Chem. Lett.* 2018, *9*, 459–463.
- (20) Zhang, W.; Kjaer, K. S.; Alonso-Mori, R.; Bergmann, U.; Chollet, M.; Fredin, L. A.; Hadt, R. G.; Hartsock, R. W.; Harlang, T.; Kroll, T.; Kubicek, K.; Lemke, H. T.; Liang, H. W.; Liu, Y.; Nielsen, M. M.; Persson, P.; Robinson, J. S.; Solomon, E. I.; Sun, Z.; Sokaras, D.; van Driel, T. B.; Weng, T.-C.; Zhu, D.; Wärnmark, K.; Sundström, V.; Gaffney, K. J. Manipulating Charge Transfer Excited State Relaxation and Spin Crossover in Iron Coordination Complexes with Ligand Substitution. *Chem. Sci.* **2017**, *8*, 515–523.
- (21) Fatur, S. M.; Shepard, S. G.; Higgins, R. F.; Shores, M. P.; Damrauer, N. H. A Synthetically Tunable System to Control MLCT Excited-State Lifetimes and Spin States in Iron(II) Polypyridines. *J. Am. Chem. Soc.* **2017**, *139*, 4493–4505.
- (22) Shepard, S. G.; Fatur, S. M.; Rappe, A. K.; Damrauer, N. H. Highly Strained Iron(II) Polypyridines: Exploiting the Quintet Manifold to Extend the Lifetime of MLCT Excited States. *J. Am. Chem. Soc.* **2016**, *138*, 2949–2952.
- (23) Mukherjee, S.; Bowman, D. N.; Jakubikova, E. Cyclometalated Fe(II) Complexes as Sensitizers in Dye-Sensitized Solar Cells. *Inorg. Chem.* **2015**, *54*, 560–569.
- (24) Bowman, D. N.; Jakubikova, E. Low-Spin Versus High-Spin Ground State in Pseudo-Octahedral Iron Complexes. *Inorg. Chem.* **2012**, *51*, 6011–6019.

(25) Dixon, I. M.; Boissard, G.; Whyte, H.; Alary, F.; Heully, J. L. Computational Estimate of the Photophysical Capabilities of Four Series of Organometallic Iron(II) Complexes. *Inorg. Chem.* **2016**, *55*, 5089–5091.

- (26) Dixon, I. M.; Khan, S.; Alary, F.; Boggio-Pasqua, M.; Heully, J. L. Probing the Photophysical Capability of Mono and Bis-(Cyclometallated) Fe(II) Polypyridine Complexes Using Inexpensive Ground State DFT. *Dalton Trans.* **2014**, *43*, 15898.
- (27) Dixon, I. M.; Alary, F.; Boggio-Pasqua, M.; Heully, J. L. The  $(N_4C_2)^{2^-}$  Donor Set as Promising Motif for Bis(Tridentate) Iron(II) Photoactive Compounds. *Inorg. Chem.* **2013**, *52*, 13369–13374.
- (28) de Graaf, C.; Sousa, C. Study of the Light-Induced Spin Crossover Process of the  $[Fe^{II}(Bpy)_3]^{2+}$  Complex. *Chem. Eur. J.* **2010**, *16*, 4550–4556.
- (29) Graaf, C. D.; Sousa, C. On the Role of the Metal-to-Ligand Charge Transfer States in the Light-Induced Spin Crossover in Fe<sup>II</sup>(bpy)<sub>3</sub>. *Int. J. Quantum Chem.* **2011**, *111*, 3385–3393.
- (30) Sousa, C.; de Graaf, C.; Rudavskyi, A.; Broer, R.; Tatchen, J.; Etinski, M.; Marian, C. M. Ultrafast Deactivation Mechanism of the Excited Singlet in the Light-Induced Spin Crossover of [Fe(2,2'-bipyridine)<sub>3</sub>]<sup>2+</sup>. *Chem. Eur. J.* **2013**, *19*, 17541–17551.
- (31) Canton, S. E.; Zhang, X.; Lawson Daku, M. L.; Liu, Y.; Zhang, J.; Alvarez, S. Mapping the Ultrafast Changes of Continuous Shape Measures in Photoexcited Spin Crossover Complexes without Long-Range Order. *J. Phys. Chem. C* **2015**, *119*, 3322–3330.
- (32) Nance, J.; Bowman, D. N.; Mukherjee, S.; Kelley, C. T.; Jakubikova, E. Insights into the Spin-State Transitions in [Fe(tpy)<sub>2</sub>]<sup>2+</sup>: Importance of the Terpyridine Rocking Motion. *Inorg. Chem.* **2015**, 54, 11259–11268.
- (33) Pápai, M.; Vankó, G.; de Graaf, C.; Rozgonyi, T. Theoretical Investigation of the Electronic Structure of Fe(II) Complexes at Spin-State Transitions. *J. Chem. Theory Comput.* **2013**, *9*, 509–519.
- (34) Jiang, Y.; Liu, L. C.; Müller-Werkmeister, H. M.; Lu, C.; Zhang, D.; Field, R. L.; Sarracini, A.; Moriena, G.; Collet, E.; Miller, R. J. D. Structural Dynamics Upon Photoexcitation in a Spin Crossover Crystal Probed with Femtosecond Electron Diffraction. *Angew. Chem., Int. Ed.* **2017**, *56*, 7130–7134.
- (35) Bailar, J. C. Some Problems in the Stereochemistry of Coordination Compounds. J. Inorg. Nucl. Chem. 1958, 8, 165–175.
- (36) Ray, P.; Dutt, N. Kinetics and Mechanism of Racemization of Optically Active Cobaltic Trisbiguanide Complex. *J. Indian Chem. Soc.* **1943**, *20*, 81–92.
- (37) Fleischer, E. B.; Gebala, A. E.; Swift, D. R.; Tasker, P. A. Trigonal Prismatic-Octahedral Coordination. Complexes of Intermediate Geometry. *Inorg. Chem.* **1972**, *11*, 2775–2784.
- (38) Wentworth, R. A. D. Trigonal Prismatic vs. Octahedral Stereochemistry in Complexes Derived from Innocent Ligands. *Coord. Chem. Rev.* **1972**, *9*, 171–187.
- (39) Purcell, K. F. Pseudorotational Intersystem Crossing in d<sup>6</sup> Complexes. J. Am. Chem. Soc. 1979, 101, 5147–5152.
- (40) Vanquickenborne, L. G.; Pierloot, K. Role of Spin Change in the Stereomobile Reactions of Strong-Field d<sup>6</sup> Transition-Metal Complexes. *Inorg. Chem.* **1981**, *20*, 3673–3677.
- (41) Comba, P.; Sargeson, A. M.; Engelhardt, L. M.; Harrowfield, J. M.; White, A. H.; Horn, E.; Snow, M. R. Analysis of Trigonal-Prismatic and Octahedral Preferences in Hexaamine Cage Complexes. *Inorg. Chem.* 1985, 24, 2325–2327.
- (42) Comba, P. Coordination Geometries of Hexaamine Cage Complexes. *Inorg. Chem.* **1989**, 28, 426–431.
- (43) McCusker, J. K.; Rheingold, A. L.; Hendrickson, D. N. Variable-Temperature Studies of Laser-Initiated  $^5T_2 \rightarrow ^1A_1$  Intersystem Crossing in Spin-Crossover Complexes: Empirical Correlations between Activation Parameters and Ligand Structure in a Series of Polypyridyl Ferrous Complexes. *Inorg. Chem.* 1996, 35, 2100–2112.
- (44) Alvarez, S. Relationships between Temperature, Magnetic Moment, and Continuous Symmetry Measures in Spin Crossover Complexes. J. Am. Chem. Soc. 2003, 125, 6795–6802.
- (45) Cremades, E.; Echeverría, J.; Alvarez, S. The Trigonal Prism in Coordination Chemistry. *Chem. Eur. J.* **2010**, *16*, 10380–10396.

(46) Knight, J. C.; Alvarez, S.; Amoroso, A. J.; Edwards, P. G.; Singh, N. A Novel Bipyridine-Based Hexadentate Tripodal Framework with a Strong Preference for Trigonal Prismatic Co-Ordination Geometries. *Dalton Trans.* **2010**, *39*, 3870–3883.

- (47) Alvarez, S. Distortion Pathways of Transition Metal Coordination Polyhedra Induced by Chelating Topology. *Chem. Rev.* **2015**, *115*, 13447–13483.
- (48) Stock, P.; Deck, E.; Hohnstein, S.; Korzekwa, J.; Meyer, K.; Heinemann, F. W.; Breher, F.; Horner, G. Molecular Spin Crossover in Slow Motion: Light-Induced Spin-State Transitions in Trigonal Prismatic Iron(II) Complexes. *Inorg. Chem.* **2016**, *55*, 5254–5265.
- (49) Montgomery, C. D.; Shorrock, C. J. Molecular Modeling Studies of the Intramolecular Twist Mechanisms of Racemization for Tris Chelate Complexes. *Inorg. Chim. Acta* **2002**, 328, 259–262.
- (50) Purcell, K. F.; Zapata, J. P. Magnetic Isomers. *cis*-Bis-(cyanotriphenylborato)bisphenanthrolineiron(II). *J. Chem. Soc., Chem. Commun.* **1978**, 497–499.
- (51) Davis, A. V.; Firman, T. K.; Hay, B. P.; Raymond, K. N., d-Orbital Effects on Stereochemical Non-Rigidity: Twisted Ti<sup>IV</sup> Intramolecular Dynamics. *J. Am. Chem. Soc.* **2006**, *128*, 9484–9496.
- (52) Rzepa, H. S.; Cass, M. E. In Search of the Bailar and Rây–Dutt Twist Mechanisms That Racemize Chiral Trischelates: A Computational Study of Sc<sup>III</sup>, Ti<sup>IV</sup>, Co<sup>III</sup>, Zn<sup>II</sup>, Ga<sup>III</sup>, and Ge<sup>IV</sup> Complexes of a Ligand Analogue of Acetylacetonate. *Inorg. Chem.* **2007**, *46*, 8024–
- (53) Amati, M.; Lelj, F. Monomolecular Isomerization Processes of Aluminum Tris(8-Hydroxyquinolinate) (Alq3): A DFT Study of Gas-Phase Reaction Paths. *Chem. Phys. Lett.* **2002**, *363*, 451–457.
- (54) Becke, A. D. Density-Functional Exchange-Energy Approximation with Correct Asymptotic Behavior. *Phys. Rev. A: At., Mol., Opt. Phys.* **1988**, 38, 3098–3100.
- (55) Lee, C.; Yang, W.; Parr, R. G. Development of the Colle-Salvetti Correlation-Energy Formula into a Functional of the Electron Density. *Phys. Rev. B: Condens. Matter Mater. Phys.* **1988**, *37*, 785–789.
- (56) Becke, A. D. Density-Functional Thermochemistry. III. The Role of Exact Exchange. *J. Chem. Phys.* **1993**, *98*, 5648–5652.
- (57) Becke, A. D. A New Mixing of Hartree–Fock and Local Density-Functional Theories. *J. Chem. Phys.* **1993**, 98, 1372.
- (58) Grimme, S. Semiempirical GGA-Type Density Functional Constructed with a Long-Range Dispersion Correction. *J. Comput. Chem.* **2006**, *27*, 1787–1799.
- (59) Dolg, M.; Wedig, U.; Stoll, H.; Preuss, H. Energy-Adjusted Ab Initio Pseudopotentials for the First Row Transition Elements. *J. Chem. Phys.* **1987**, *86*, 866–872.
- (60) Krishnan, R.; Binkley, J. S.; Seeger, R.; Pople, J. A. Self-Consistent Molecular Orbital Methods. XX. A Basis Set for Correlated Wave Functions. *J. Chem. Phys.* **1980**, *72*, 650–654.
- (61) Grimme, S.; Antony, J.; Ehrlich, S.; Krieg, H. A Consistent and Accurate Ab Initio Parametrization of Density Functional Dispersion Correction (DFT-D) for the 94 Elements H-Pu. *J. Chem. Phys.* **2010**, 132, 154104.
- (62) Salomon, O.; Reiher, M.; Hess, B. A. Assertion and Validation of the Performance of the B3LYP\* Functional for the First Transition Metal Row and the G2 Test Set. *J. Chem. Phys.* **2002**, *117*, 4729–4737.
- (63) Reiher, M. Theoretical Study of the Fe(phen)<sub>2</sub>(NCS)<sub>2</sub> Spin-Crossover Complex with Reparametrized Density Functionals. *Inorg. Chem.* **2002**, *41*, 6928–6935.
- (64) Reiher, M.; Salomon, O.; Artur Hess, B. Reparameterization of Hybrid Functionals Based on Energy Differences of States of Different Multiplicity. *Theor. Chem. Acc.* **2001**, *107*, 48–55.
- (65) The parameters employed here for the D2 correction were the same as those derived for B3LYP.
- (66) Tao, J.; Perdew, J. P.; Staroverov, V. N.; Scuseria, G. E. Climbing the Density Functional Ladder: Nonempirical Meta-Generalized Gradient Approximation Designed for Molecules and Solids. *Phys. Rev. Lett.* **2003**, *91*, 146401.
- (67) Staroverov, V. N.; Scuseria, G. E.; Tao, J.; Perdew, J. P. Erratum: "Comparative Assessment of a New Nonempirical Density Functional:

Molecules and Hydrogen-Bonded Complexes" [J. Chem. Phys. 119, 12129 (2003)]. J. Chem. Phys. 2004, 121, 11507–11507.

- (68) Staroverov, V. N.; Scuseria, G. E.; Tao, J.; Perdew, J. P. Comparative Assessment of a New Nonempirical Density Functional: Molecules and Hydrogen-Bonded Complexes. *J. Chem. Phys.* **2003**, *119*, 12129–12137.
- (69) Perdew, J. P. Density-Functional Approximation for the Correlation Energy of the Inhomogeneous Electron Gas. *Phys. Rev. B: Condens. Matter Mater. Phys.* 1986, 33, 8822–8824.
- (70) Zhao, Y.; Truhlar, D. G. The M06 Suite of Density Functionals for Main Group Thermochemistry, Thermochemical Kinetics, Noncovalent Interactions, Excited States, and Transition Elements: Two New Functionals and Systematic Testing of Four M06-Class Functionals and 12 Other Functionals. *Theor. Chem. Acc.* 2008, 120, 215–241.
- (71) Zhao, Y.; Truhlar, D. G. A New Local Density Functional for Main-Group Thermochemistry, Transition Metal Bonding, Thermochemical Kinetics, and Noncovalent Interactions. *J. Chem. Phys.* **2006**, *125*, 194101.
- (72) Austin, A.; Petersson, G. A.; Frisch, M. J.; Dobek, F. J.; Scalmani, G.; Throssell, K. A Density Functional with Spherical Atom Dispersion Terms. *J. Chem. Theory Comput.* **2012**, *8*, 4989–5007.
- (73) Frisch, M. J.; Trucks, G. W.; Schlegel, H. B.; Scuseria, G. E.; Robb, M. A.; Cheeseman, J. R.; Scalmani, G.; Barone, V.; Mennucci, B.; Petersson, G. A.; Nakatsuji, H.; Caricato, M.; Li, X.; Hratchian, H. P.; Izmaylov, A. F.; Bloino, J.; Zheng, G.; Sonnenberg, J. L.; Hada, M.; Ehara, M.; Toyota, K.; Fukuda, R.; Hasegawa, J.; Ishida, M.; Nakajima, T.; Honda, Y.; Kitao, O.; Nakai, H.; Vreven, T.; Montgomery, J. A., Jr.; Peralta, J. E.; Ogliaro, F.; Bearpark, M.; Heyd, J. J.; Brothers, E.; Kudin, K. N.; Staroverov, V. N.; Kobayashi, R.; Normand, J.; Raghavachari, K.; Rendell, A.; Burant, J. C.; lyengar, S. S.; Tomasi, J.; Cossi, M.; Rega, N.; Millam, N. J.; Klene, M.; Knox, J. E.; Cross, J. B.; Bakken, V.; Adamo, C.; Jaramillo, J.; Gomperts, R.; Stratmann, R. E.; Yazyev, O.; Austin, A. J.; Cammi, R.; Pomelli, C.; Ochterski, J. W.; Martin, R. L.; Morokuma, K.; Zakrzewski, V. G.; Voth, G. A.; Salvador, P.; Dannenberg, J. J.; Dapprich, S.; Daniels, A. D.; Farkas, Ö.; Foresman, J. B.; Ortiz, J. V.; Cioslowski, J.; Fox, D. J.; Gaussian 09, revision D.01; Gaussian, Inc.: Wallingford, CT, 2009.
- (74) Valiev, M.; Bylaska, E. J.; Govind, N.; Kowalski, K.; Straatsma, T. P.; Van Dam, H. J. J.; Wang, D.; Nieplocha, J.; Apra, E.; Windus, T. L.; de Jong, W. A. NWChem: A Comprehensive and Scalable Open-Source Solution for Large Scale Molecular Simulations. *Comput. Phys. Commun.* **2010**, *181*, 1477–1489.
- (75) Roos, B. O.; Taylor, P. R.; Siegbahn, P. E. M. A Complete Active Space SCF Method (CASSCF) Using a Density Matrix Formulated Super-CI Approach. *Chem. Phys.* **1980**, *48*, 157–173.
- (76) Siegbahn, P.; Heiberg, A.; Roos, B.; Levy, B. A Comparison of the Super-CI and the Newton-Raphson Scheme in the Complete Active Space SCF Method. *Phys. Scr.* **1980**, *21*, 323.
- (77) Siegbahn, P. E. M.; Almlöf, J.; Heiberg, A.; Roos, B. O. The Complete Active Space SCF (CASSCF) Method in a Newton–Raphson Formulation with Application to the HNO Molecule. *J. Chem. Phys.* **1981**, *74*, 2384–2396.
- (78) Neese, F. The Orca Program System. Wiley Interdiscip. Rev.: Comput. Mol. Sci. 2012, 2, 73–78.
- (79) Pantazis, D. A.; Chen, X.-Y.; Landis, C. R.; Neese, F. All-Electron Scalar Relativistic Basis Sets for Third-Row Transition Metal Atoms. *J. Chem. Theory Comput.* **2008**, *4*, 908–919.
- (80) Weigend, F.; Ahlrichs, R. Balanced Basis Sets of Split Valence, Triple Zeta Valence and Quadruple Zeta Valence Quality for H to Rn: Design and Assessment of Accuracy. *Phys. Chem. Chem. Phys.* **2005**, *7*, 3297–3305.
- (81) Hess, B. A. Relativistic Electronic-Structure Calculations Employing a Two-Component No-Pair Formalism with External-Field Projection Operators. *Phys. Rev. A: At., Mol., Opt. Phys.* **1986**, 33, 3742–3748.
- (82) Neese, F.; Wennmohs, F.; Hansen, A.; Becker, U. Efficient, Approximate and Parallel Hartree-Fock and Hybrid DFT Calcu-

lations. A 'Chain-of-Spheres' Algorithm for the Hartree-Fock Exchange. *Chem. Phys.* **2009**, *356*, 98–109.

- (83) Izsák, R.; Neese, F. An Overlap Fitted Chain of Spheres Exchange Method. *J. Chem. Phys.* **2011**, *135*, 144105.
- (84) Weigend, F. Hartree-Fock Exchange Fitting Basis Sets for H to Rn. J. Comput. Chem. 2008, 29, 167–175.
- (85) Hoffmann, R.; Howell, J. M.; Rossi, A. R. Bicapped Tetrahedral, Trigonal Prismatic, and Octahedral Alternatives in Main and Transition Group Six-Coordination. *J. Am. Chem. Soc.* **1976**, 98, 2484–2492.
- (86) Angeli, C.; Cimiraglia, R.; Malrieu, J.-P. N-Electron Valence State Perturbation Theory: A Spinless Formulation and an Efficient Implementation of the Strongly Contracted and of the Partially Contracted Variants. *J. Chem. Phys.* **2002**, *117*, 9138.
- (87) Angeli, C.; Cimiraglia, R.; Malrieu, J.-P. N-Electron Valence State Perturbation Theory: A Fast Implementation of the Strongly Contracted Variant. *Chem. Phys. Lett.* **2001**, *350*, 297–305.
- (88) Angeli, C.; Cimiraglia, R.; Evangelisti, S.; Leininger, T.; Malrieu, J. P. Introduction of N-Electron Valence States for Multireference Perturbation Theory. *J. Chem. Phys.* **2001**, *114*, 10252.
- (89) Angeli, C.; Cimiraglia, R. Multireference Perturbation Configuration Interaction V. Third-Order Energy Contributions in the Møller–Plesset and Epstein–Nesbet Partitions. *Theor. Chem. Acc.* **2002**, *107*, 313–317.
- (90) Pierloot, K.; Phung, Q. M.; Domingo, A. Spin State Energetics in First-Row Transition Metal Complexes: Contribution of (3s3p) Correlation and Its Description by Second-Order Perturbation Theory. *J. Chem. Theory Comput.* **2017**, *13*, 537–553.
- (91) Freitag, L.; Knecht, S.; Angeli, C.; Reiher, M. Multireference Perturbation Theory with Cholesky Decomposition for the Density Matrix Renormalization Group. *J. Chem. Theory Comput.* **2017**, *13*, 451.
- (92) Queralt, N.; Taratiel, D.; de Graaf, C.; Caballol, R.; Cimiraglia, R.; Angeli, C. On the Applicability of Multireference Second-Order Perturbation Theory to Study Weak Magnetic Coupling in Molecular Complexes. *J. Comput. Chem.* **2008**, *29*, 994–1003.
- (93) Heilmann, J.; Lerner, H.-W.; Bolte, M. Tris(2,2'-Bipyridyl)-Iron(II) Dibromide 4.5-Hydrate. *Acta Crystallogr., Sect. E: Struct. Rep.* **2006**, 62, m1477—m1478.
- (94) Hauser, A.; Enachescu, C.; Daku, M. L.; Vargas, A.; Amstutz, N. Low-Temperature Lifetimes of Metastable High-Spin States in Spin-Crossover and in Low-Spin Iron(II) Compounds: The Rule and Exceptions to the Rule. *Coord. Chem. Rev.* **2006**, *250*, 1642–1652.
- (95) The Bailar twist itself is, of course, named after John C. Bailar, Jr., the famous inorganic chemist. Note that, in addition to being an aesthetically appropriate descriptor for our structure, the word for "dance" in Spanish is "bailar".
- (96) Bhattacharyya, K.; Surendran, A.; Chowdhury, C.; Datta, A. Steric and Electric Field Driven Distortions in Aromatic Molecules: Spontaneous and Non-Spontaneous Symmetry Breaking. *Phys. Chem. Chem. Phys.* **2016**, *18*, 31160–31167.
- (97) Pratik, S. M.; Chowdhury, C.; Bhattacharjee, R.; Jahiruddin, S.; Datta, A. Pseudo Jahn—Teller Distortion for a Tricyclic Carbon Sulfide  $(C_6S_8)$  and Its Suppression in S-Oxygenated Dithiine  $(C_4H_4(SO_2)_2)$ . Chem. Phys. **2015**, 460, 101–105.
- (98) Pearson, R. G. Symmetry Rule for Predicting Molecular Structures. J. Am. Chem. Soc. 1969, 91, 4947–4955.
- (99) Ashley, D. C.; Baik, M.-H. The Electronic Structure of [Mn(V)=O]: What Is the Connection between Oxyl Radical Character, Physical Oxidation State, and Reactivity? *ACS Catal.* **2016**, *6*, 7202–7216.
- (100) Boguslawski, K.; Jacob, C. R.; Reiher, M. Can DFT Accurately Predict Spin Densities? Analysis of Discrepancies in Iron Nitrosyl Complexes. J. Chem. Theory Comput. 2011, 7, 2740–2752.
- (101) Pierloot, K.; Zhao, H.; Vancoillie, S. Copper Corroles: The Question of Noninnocence. *Inorg. Chem.* **2010**, *49*, 10316–10329.
- (102) Venturinelli Jannuzzi, S. A.; Phung, Q. M.; Domingo, A.; Formiga, A. L. B.; Pierloot, K. Spin State Energetics and Oxyl Character of Mn-Oxo Porphyrins by Multiconfigurational Ab Initio

Calculations: Implications on Reactivity. *Inorg. Chem.* **2016**, *55*, 5168–5179.

- (103) Radoń, M.; Broclawik, E.; Pierloot, K. Electronic Structure of Selected {FeNO}<sup>7</sup> Complexes in Heme and Non-Heme Architectures: A Density Functional and Multireference Ab Initio Study. *J. Phys. Chem. B* **2010**, *114*, 1518–1528.
- (104) Fracchia, F.; Cimiraglia, R.; Angeli, C. Assessment of Multireference Perturbation Methods for Chemical Reaction Barrier Heights. *J. Phys. Chem. A* **2015**, *119*, 5490–5495.
- (10S) Braterman, P. S.; Song, J.-I.; Peacock, R. D. Electronic Absorption Spectra of the Iron(II) Complexes of 2,2-Bipyridine, 2,2'-Pipyrimidine, 1,10-Phenanthroline, and 2,2':6',2"-Terpyridine and Their Reduction Products. *Inorg. Chem.* **1992**, 31, 555–559.
- (106) Ford-Smith, M. H.; Sutin, N. The Kinetics of the Reactions of Substituted 1,10-Phenanthroline, 2,2'-Dipyridine and 2,2',2"-Tripyridine Complexes of Iron(III) with Iron(II) Ions. *J. Am. Chem. Soc.* 1961, 83, 1830–1834.
- (107) Towns, J.; Cockerill, T.; Dahan, M.; Foster, I.; Gaither, K.; Grimshaw, A.; Hazlewood, V.; Lathrop, S.; Lifka, D.; Peterson, G. D.; Roskies, R.; Scott, J. R.; Wilkens-Diehr, N. XSEDE: Accelerating Scientific Discovery. *Comput. Sci. Eng.* **2014**, *16*, 62–74.